

**The microstructural evolution and elemental distribution of a 3rd generation 1 GPa advanced high strength steel during double pulse resistance spot welding**

Eftekharimilani, Parisa; van der Aa, EM; Hermans, Marcel; Richardson, Ian

**DOI**

[10.1007/s40194-017-0459-4](https://doi.org/10.1007/s40194-017-0459-4)

**Publication date**

2017

**Document Version**

Final published version

**Published in**

Welding in the World

**Citation (APA)**

Eftekharimilani, P., van der Aa, EM., Hermans, M., & Richardson, I. (2017). The microstructural evolution and elemental distribution of a 3rd generation 1 GPa advanced high strength steel during double pulse resistance spot welding. *Welding in the World*, 61(4), 691 - 701. <https://doi.org/10.1007/s40194-017-0459-4>

**Important note**

To cite this publication, please use the final published version (if applicable). Please check the document version above.


**Copyright**

Other than for strictly personal use, it is not permitted to download, forward or distribute the text or part of it, without the consent of the author(s) and/or copyright holder(s), unless the work is under an open content license such as Creative Commons.

**Takedown policy**

Please contact us and provide details if you believe this document breaches copyrights. We will remove access to the work immediately and investigate your claim.

# The microstructural evolution and elemental distribution of a 3<sup>rd</sup> generation 1 GPa advanced high strength steel during double pulse resistance spot welding

P. Eftekharimilani<sup>1</sup>  · E. M. van der Aa<sup>2</sup> · M. J. M. Hermans<sup>1</sup> · I. M. Richardson<sup>1</sup>

Received: 5 August 2016 / Accepted: 18 March 2017

© The Author(s) 2017. This article is published with open access at Springerlink.com

**Abstract** This paper presents the effects of double pulse resistance spot welding (RSW) on the microstructural evolution, elemental distribution and mechanical properties of a 3<sup>rd</sup> generation 1 GPa advanced high strength steel (AHSS). In order to investigate the effect of double pulsing, the steel was exposed to single and various double pulse RSW schedules. The first current pulse was applied to create the weld nugget, while the second current pulse generated a secondary weld nugget and annealed or (partial) re-melted the primary weld nugget, depending on the magnitude of the current. The effect of the second current pulse on the weld nugget and heat-affected zone characteristics was investigated using optical microscopy and electron probe microanalysis (EPMA). Optical and electron microscopy revealed that the secondary weld nugget is fully martensitic, showing a typical solidification microstructure, while the annealed zone reveals an equi-axed martensitic structure. EPMA results showed that elemental segregation has been considerably reduced in the annealed zone. Mechanical properties of the welds show that the AHSS studied is prone to weld metal failure for single pulse RSW. However, the double pulse RSW method can lead to significantly improved mechanical performance and favourable failure modes.

**Keywords (IIW Thesaurus)** Resistance spot welding · Low alloy steels · Microstructure · Segregation · Mechanical properties

## 1 Introduction

The demand for the development of lighter, safer, greener and more cost-effective vehicles leads to continued development of advanced high strength steels (AHSSs) that meet functional requirements on strength and formability that allow weight reduction and provide good crashworthiness for automotive applications. In these steels, the required properties are achieved by means of multi-phase microstructures [1].

Resistance spot welding (RSW) is by far the most widely used joining method in the automotive industry due to the high operating speeds, low costs, the reliability of the process and the suitability for automation [2–4]. However, the thermal-mechanical cycle during resistance spot welding destroys the carefully designed multi-phase microstructure. The resulting weld microstructure is both chemically and mechanically heterogeneous. The high alloying content of third-generation AHSSs limit their weldability and unfavourable modes of weld failure are frequently observed [5]. The presence of a relatively high percentage of alloying elements in combination with the high cooling rates of the welding process leads to the formation of a martensitic microstructure that influences the mechanical properties of the welds. Alloying elements like silicon, manganese and phosphorous tend to segregate to the grain boundaries during solidification [6, 7]. Furthermore, the formation of non-metallic and complex inclusions is reported in the fusion zone of welded AHSSs [8–10]. Apart from the martensite, the segregation of the alloying elements and inclusions are

---

Recommended for publication by Commission III - Resistance Welding, Solid State Welding, and Allied Joining Process

✉ P. Eftekharimilani  
p.eftekharimilani@tudelft.nl

<sup>1</sup> Faculty of 3mE, Department of Materials Science and Engineering, TU Delft, 2628 CD Delft, The Netherlands

<sup>2</sup> Tata Steel, 1970 CA, IJmuiden, The Netherlands

factors that considerably influence the mechanical performance of the welds.

Post pulsing is considered one of the most effective ways in order to modify the microstructure and improve the mechanical properties of resistance spot welds [11–20]. Hernandez et al. [15] have studied the effect of second pulse current in the resistance spot-welded TRIP steels on the microstructure and its relation to the mechanical properties of the material. Van der Aa et al. [14] reported a post pulsing welding scheme for the resistance spot welding of 3<sup>rd</sup> generation AHSSs, with a significant improvement in the mechanical properties.

In this paper, a systematic study on double pulse welding is reported for a 3<sup>rd</sup> generation 1 GPa AHSS to monitor the effect of the second pulse current level on the microstructure, elemental distribution and mechanical properties of the welds. Improved welding schemes with double pulsing are derived.

## 2 Experimental procedure

A 3<sup>rd</sup> generation 1 GPa AHSS with a thickness of 1.3 mm was used in this study. The steel was received in a cold-rolled and galvanised condition (surface density of 50 g m<sup>-2</sup>). Material characteristics and composition conform to the VDA chemistry for 590Y980T-DH in the recently drafted VDA specifications and are listed in Table 1. The initial microstructure of the steel is shown in Fig. 1.

For resistance spot welding, chisel and cross tension strength (CTS) samples (Fig. 2a, b) were cut from the as-received steel plates. Resistance spot welding was carried out on a SchlattesTM 50-Hz A/C spot welding machine using F1 16 × 5.5 electrodes with a holding force of 4 kN, as described in the VDEh SEP1220-2 standard [21]. Welding parameters to construct the weld growth curve are mentioned in Table 2.  $I_{\min}$  is the weld current needed to produce a  $4.25\sqrt{t}$  weld nugget diameter, where  $t$  is the sheet thickness and  $I_{\max}$  is the highest current amplitude before splashing occurs. The welding parameters used to produce welds for microstructural characterisation, elemental analyses, hardness and mechanical measurements are shown in Table 3. Sequence 1 is a single pulse resistance spot weld. Apart from the standard single pulse weld scheme, several double pulse weld schemes were applied, with a systematic variation of the second pulse

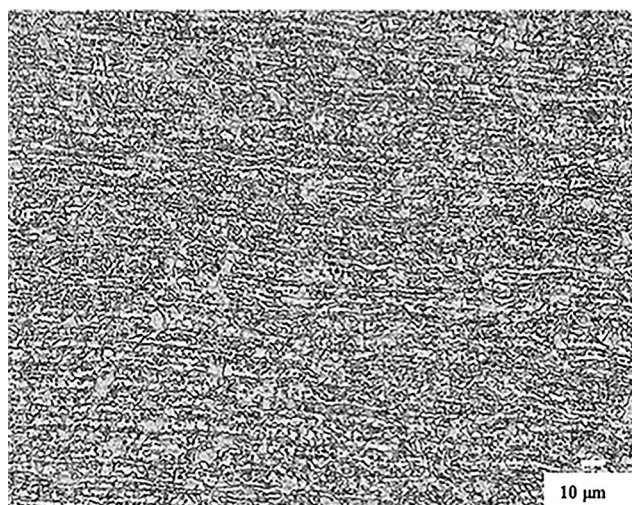


Fig. 1 Base material microstructure of 3<sup>rd</sup> generation 1 GPa AHSS

current level. Sequence 2 is a double pulse resistance spot weld with the second pulse current about 8% lower than the first pulse current. In sequence 3, two equal pulse currents in double pulse resistance spot welding were used. Sequence 4 is produced using a second pulse current about 11% higher than the first one. The cool time of 40 ms is chosen to allow the weld edge to remain austenitic between two pulses and obtain more equi-axed prior austenite grains. This specific time is selected with regard to the prior SORPAS simulations of temperature-time profiles at the weld edge [22]. From a practical point of view, extending the total thermal cycle time is not preferred. The welding schemes are indicated schematically in Fig. 3a, b.

The weld growth analysis was carried out for the single pulse welding scheme using chisel test specimens. The failure modes of these welds were investigated by optical microscopy and visual inspection. The weld nugget size and plug diameter were measured to obtain the weld growth curves and plug ratios, respectively. The plug ratio (ratio of plug diameter to weld nugget size) was calculated to analyse the partial plug failures.

For optical microscopy analysis, the sheets were cross-sectioned, polished and etched with 4% Nital solution for 5 s. To reveal dendrites and prior austenite grain boundaries at the weld nugget and HAZ of the welds, an etchant consisting of 1% aqueous solution of sodium dodecylbenzenesulfonate and

Table 1 Material characteristics

Thickness (mm)	Proof strength/ultimate tensile strength (MPa)	Elongation at fracture L0 = 80 mm (%)	C (wt%)	Mn (wt%)	Si (wt%)	Al (wt%)	Cr + Mo (wt%)
1.3	≥590/≥980	≥15	≤0.22	≤2.9	≤1.9	0.015–1.0	≤1.40

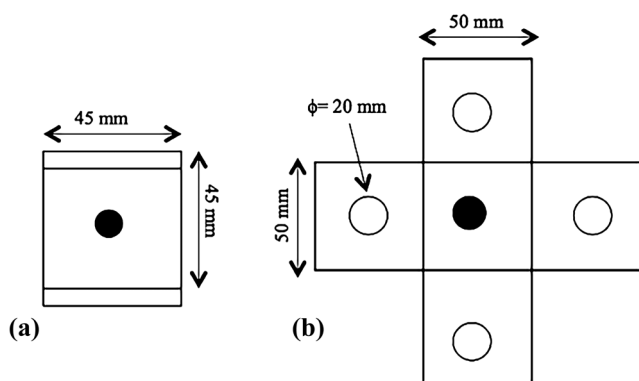


**Fig. 2** Schematic representation of the samples for **a** chisel test and **b** cross tension strength test

4% picric acid in ethanol was used. Microstructural analysis was carried out using a Keyence VHX Multi Scan Digital microscope. Quantitative elemental distributions at the weld edges of resistance spot welds were determined by electron probe microanalysis (EPMA). The measurements were performed with a Cameca SX100 microprobe, using an electron beam with an energy of 15 keV and a beam current of 100 nA, employing wavelength dispersive spectroscopy (WDS). The composition at each analysis location was determined using the X-ray intensities of the constituent elements after background correction relative to the corresponding intensities of reference materials. The intensities were processed with a phi-rho-z matrix correction program from Cameca. Analyses were made on  $200 \times 200 \mu\text{m}^2$  areas near the weld edges with a step size of  $1 \mu\text{m}$  and a counting time of 1 s per point.

Mechanical properties of the welds were evaluated by standard CTS tests (Fig. 2b) [21]. The CTS tests were repeated three times for each welding sequence. Load-displacement curves, average maximum force and elongation at the maximum load were recorded for the samples during testing. The weld nugget size and plug diameter were also measured for CTS samples with a calliper. Vickers microhardness measurements with a load of 500 g and a dwell time of 10 s were performed.

**Table 2** Resistance spot welding parameters for determining the weld growth curves

	Minimum weld nugget size ( $4.25 \times \sqrt{t}$ ) (mm)	Squeeze time (ms)	Weld time (ms)	Hold time (ms)	$I_{\min}$ (kA)	$I_{\max}$ (kA)
3 <sup>rd</sup> generation 1 GPa AHSS	4.8	400	320	200	5.7	7.5

## 3 Results

### 3.1 Weld growth curves

The weld growth curves for the 3<sup>rd</sup> generation 1 GPa AHSS obtained from experimental investigation are plotted in Fig. 4. The weld nugget sizes range from 5.0 to 6.6 mm. Splashing occurs at current levels above 7.5 kA. In this study, the primary welding currents of 6.2 kA were selected. This current leads to a weld nugget diameter of 5.2 mm.

### 3.2 Microstructural characterisation

A schematic representation of a cross section of a double pulse weld is shown in Fig. 5. During the first pulse, the primary weld nugget is produced. The second pulse results in a re-melted zone inside the primary weld nugget, forming a secondary weld nugget.

Cross section macrographs of the single and double pulse resistance spot welded 3<sup>rd</sup> generation 1 GPa AHSS are shown in Fig. 6. The weld nugget diameters obtained from metallographic investigation are shown in Table 4. It should be noted that the exact location of cross sectioning affects the measured weld nugget size obtained by metallographic analysis. In all the samples, the fusion zone, heat-affected zone and base material can be distinguished. The weld nugget of the single pulse weld (sequence 1 in Table 3) contains a typical columnar solidification structure (Fig. 6a). Within the primary weld nugget, a secondary nugget can be observed when sequences 2 or 3 is employed. The secondary weld nugget diameter of sequence 3 is larger than sequence 2 (Table 4). If the second pulse current level is further increased, the diameter of secondary weld nugget is larger than the first one (Fig. 6d).

The secondary weld nugget shows a martensitic solidification structure (Fig. 7a). The annealed zones in sequences 2 and 3 also show martensite. However, the martensitic structure in this area is equi-axed (Fig. 7b). Detailed images of the dendrites and equi-axed grains are shown in Fig. 8. Dendrites with a typical solidification grain orientation at the weld nugget of a resistance spot weld are shown in Fig. 8a and are depicted with higher magnification in Fig. 8b. The annealed zone of a double pulse weld reveals prior austenite grains with an equi-axed grain structure (Fig. 8c, d). The existence of dendrites in some equi-axed grains at the interface of the secondary weld nugget and the annealed zone indicates partial re-melting during the second current pulse (Fig. 8d).

### 3.3 Elemental distribution

The measured elemental distribution for manganese, silicon and phosphorus at the weld edges of the primary weld nugget is shown in Figs. 9, 10 and 11, respectively. The solidification structure is obvious for sequences 1 and 4 and the strong

**Table 3** Single and double pulse resistance spot welding parameters

Sequence	No. of pulses	Squeeze time (ms)	Weld time 1 (ms)	Current 1 (kA)	Cool time (ms)	Current 2 (kA)	Weld time 2 (ms)	Hold time (ms)
1	1	400	320	6.2	–	–	–	200
2	2	400	320	6.2	40	5.7	320	200
3	2	400	320	6.2	40	6.2	320	200
4	2	400	320	6.2	40	6.9	320	200

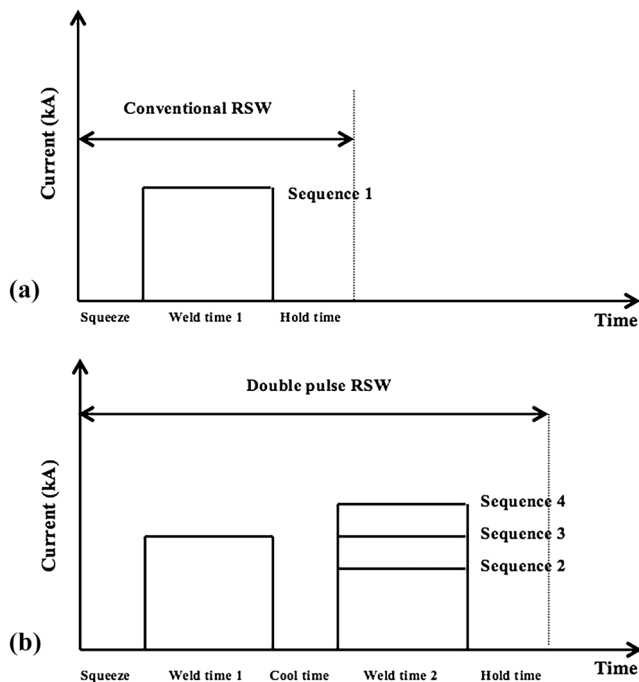
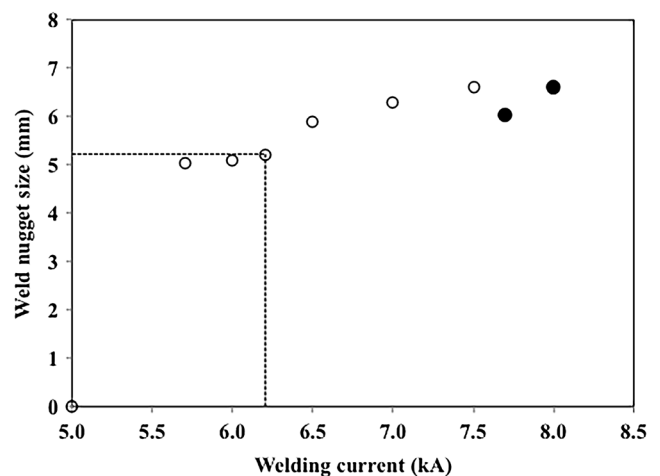
segregations of manganese, silicon and phosphorus are clear (Figs. 9a,d, 10aa,d and 11a, d). In sequence 2, the elemental segregations have been reduced in comparison with sequences 1 and 4. The distribution of manganese, silicon and phosphorus for this weld shows the presence of the elements at prior austenite grain boundaries as well as within the dendrite structure in some areas. Homogenising of the alloying elements during the second current pulse has occurred. The EPMA plots for sequence 3 show the lowest segregation of elements (Figs. 9c, 10ca and 11c). In this weld, like sequence 2, homogenisation of alloying elements has taken place and in just a few zones in the EPMA plots, the prior austenite grain boundaries can be seen, i.e. the areas with higher concentrations of manganese, silicon and phosphorus. Further quantitative study of the elemental segregation for different welds was done with line scans taken vertically at approximately 25  $\mu\text{m}$  from the right-hand side of the elemental plots. The line scans and the average and standard deviation of the results are presented in

Fig. 12 and Table 5, respectively. The quantitative results of the line scans (Table 5) show that the lowest segregation of the elements is related to sequence 3, which was welded with two equal pulse currents.

### 3.4 Mechanical properties

The microhardness profiles of the 3<sup>rd</sup> generation 1 GPa AHSS welds subjected to different welding schemes are shown in Fig. 13. The average weld nugget microhardness of sequence 1 is about 500 HV<sub>500g</sub>. For double pulse spot welds, different pulse currents do not significantly influence the hardness of the welds.

The cross tension strengths for the single and double pulse welds are shown in Fig. 14 and the measured properties are provided in Table 6. The double pulse welds show higher force and displacement in comparison with the single pulse weld. The double pulse weld, which is welded with two equal pulses (sequence 3), shows the highest force and displacement. The measured weld nugget sizes show that the sequences 1 to 3 have similar weld nugget diameters. However, sequence 4 has a larger weld nugget size due to the high current in the second weld pulse (Table 6). Even with the wider weld nugget and HAZ widths after sequence 4, the

**Fig. 3** Schematic representation of **a** the conventional and **b** the double pulse RSW schemes**Fig. 4** Weld growth curve for the 3<sup>rd</sup> generation 1 GPa AHSS. The *solid symbols* indicate splashing

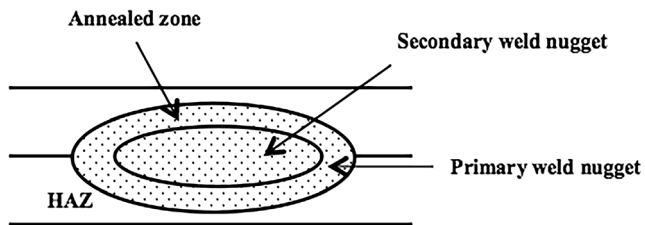


**Fig. 5** Schematic representation of the primary and secondary weld nugget of a weld subjected to double pulse RSW. The dotted area is the primary weld nugget

CTS strength of the welds made with sequence 4 are clearly lower than for sequence 3 (Fig. 14). The addition of the second current pulse leads to an increase in the bearing force and displacement of the welds.

## 4 Discussion

In the preceding sections, the microstructural evolution, elemental distribution and the mechanical properties of 3<sup>rd</sup> generation 1 GPa AHSS subjected to single and double pulse RSW have been reported.

### 4.1 Microstructural characterisation

During conventional RSW, a weld nugget is formed, the size of which depends on the welding current applied (Fig. 4). The single pulse weld (sequence 1) shows typical martensitic solidification structure inside the weld nugget due to the high cooling rate during RSW. As schematically shown in Fig. 5, the welds subjected to double pulse RSW show two distinct weld nuggets. The primary weld nugget is generated during

**Table 4** Weld nugget diameters for different sequences obtained from metallography investigation

Sequence	1	2	3	4
Primary weld nugget size (mm)	5.1	5.2	5.2	–
Secondary weld nugget size (mm)	–	3.7	4.3	5.7

the first pulse and the secondary weld nugget is a re-melted zone inside the primary weld nugget as a result of second pulse current. The secondary weld nugget shows dendritic structure similar to single pulse weld (sequence 1). The zone between the primary and secondary weld nuggets is annealed and differs in size and microstructure for different welds according to the magnitude of the second pulse current (Fig. 6). The annealed zone consists of martensitic microstructure with equi-axed grains (Figs. 7 and 8). Previous study [22] showed that during second pulse welding, solid-state phase transformation (austenitisation) occurs at the weld edge of the sequences 2 and 3 welds. In case of sequence 4, second pulse welding re-melts the primary weld nugget and creates a nugget larger than the primary weld. The replacement of the dendritic structure at the weld edge of the sequences 2 and 3 with equi-axed grains (prior austenite grains) as a result of double pulse welding could be one of the important effects of pulse welding on the microstructure.

### 4.2 Elemental distribution

The elemental partitioning at the weld edge is one of the most important factors in defining the mechanical

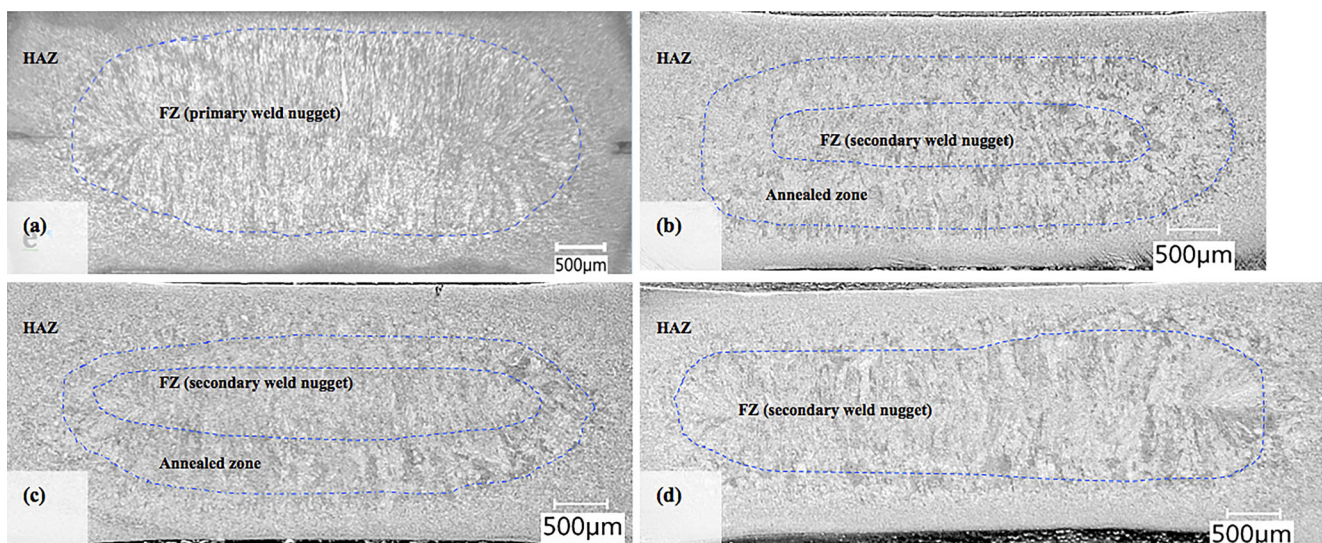


**Fig. 6** Macrographs of the cross sections of the resistance spot welded **a** sequence 1, **b** sequence 2 (5.7 kA), **c** sequence 3 (6.2 kA) and **d** sequence 4 (6.9 kA)

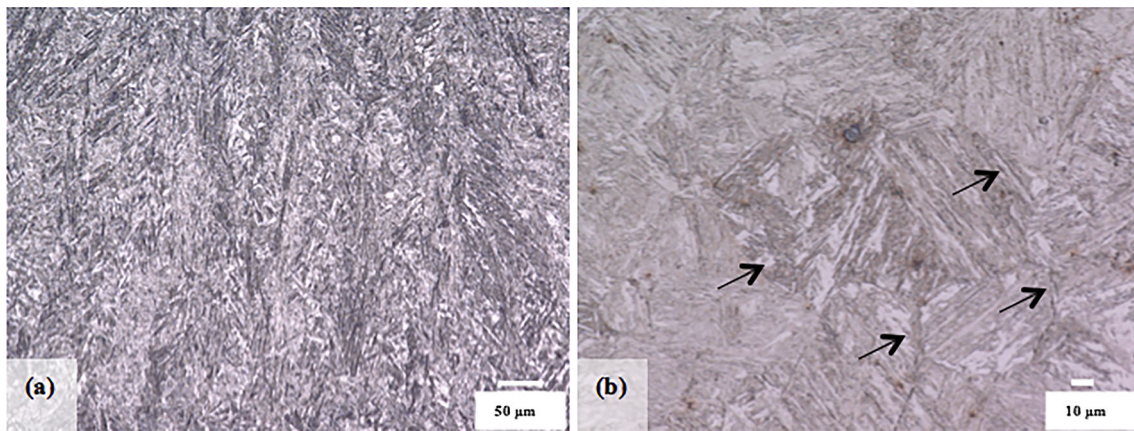


**Fig. 7** Micrographs of a cross section of the sequence 2, **a** secondary weld nugget showing solidification dendritic structure and **b** annealed zone showing equi-axed grains (*arrows* show the grain boundaries)

properties of the resistance spot welds [23]. The EPMA measurements show strong segregation of alloying elements such as manganese, silicon and phosphorus at the weld edge of the sequence 1 (single pulse weld). The elemental segregation has taken place at the dendritic boundaries (Fig. 9a, 10a and 11a). The results of the elemental plots and line scans reveal that elemental

partitioning has been considerably reduced in sequences 2 and 3 (Fig. 9b, c, 10b,c and 11b, c). The homogenisation of alloying elements is the result of annealing of the weld edge during the second current pulse. In sequence 2, the second current pulse has annealed the weld edge and austenite grain growth took place and as a result homogenisation of manganese, silicon and

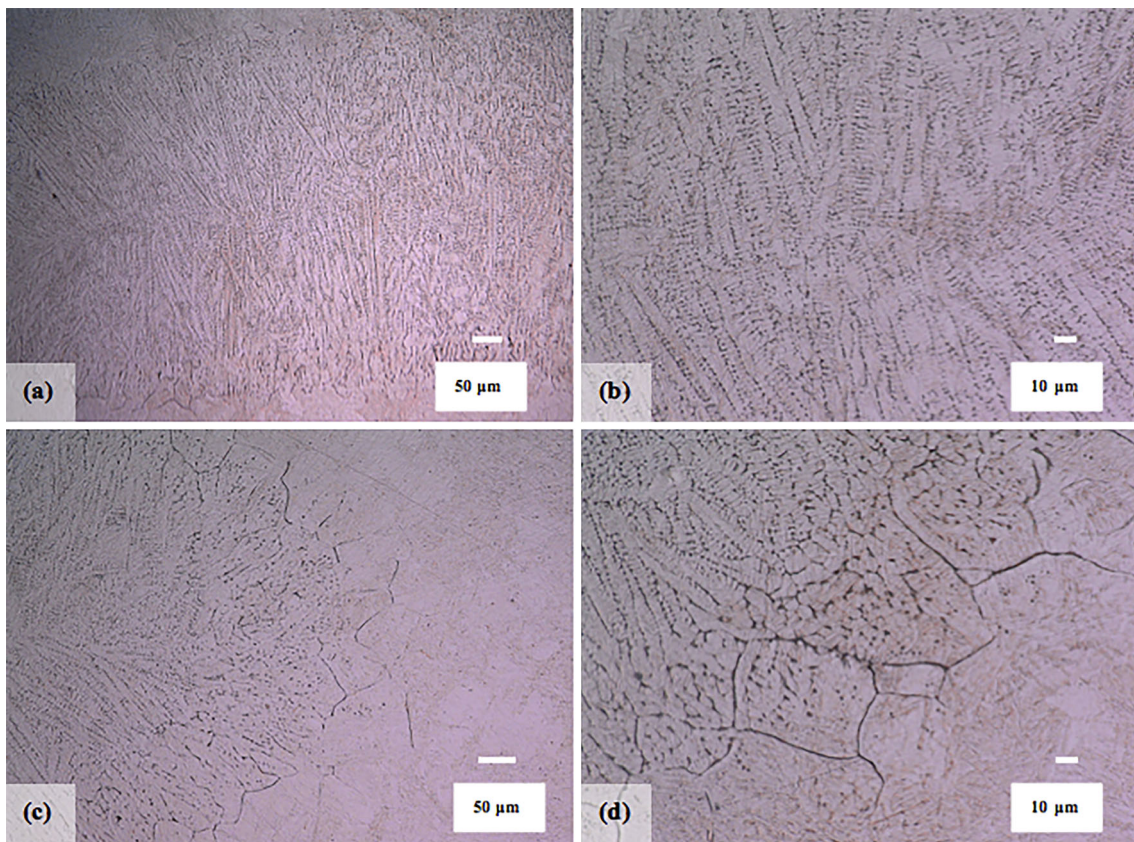


**Fig. 8** Micrographs of the cross sections of a double pulse welds (sequence 3) using improved etchant, **a** secondary weld nugget, **b** higher magnification of secondary weld nugget, showing dendritic structure, **c** annealed zone and **d** higher magnification of the annealed zone showing equi-axed grains

**Fig. 9** Elemental maps of manganese, taken at the edge of the primary weld nugget **a** sequence 1, **b** sequence 2 (5.7 kA), **c** sequence 3 (6.2 kA) and **d** sequence 4 (6.9 kA)

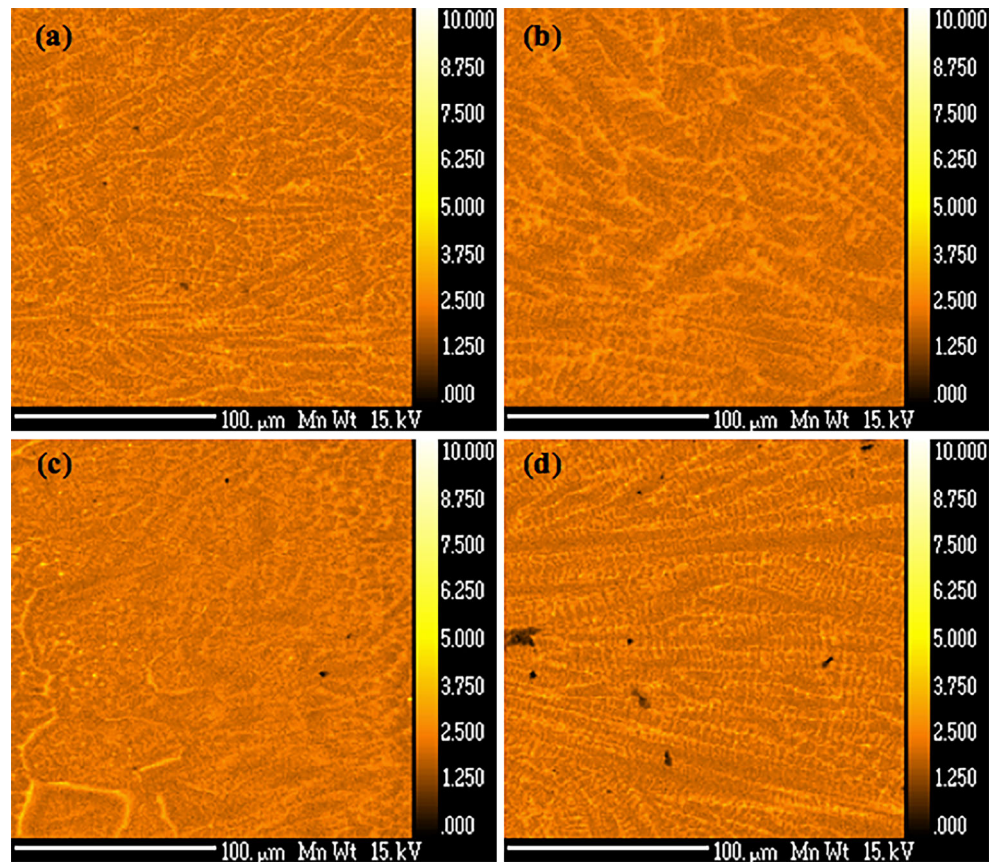


**Fig. 10** Elemental maps of silicon, taken at the edge of the primary weld nugget **a** sequence 1, **b** sequence 2 (5.7 kA), **c** sequence 3 (6.2 kA) and **d** sequence 4 (6.9 kA)

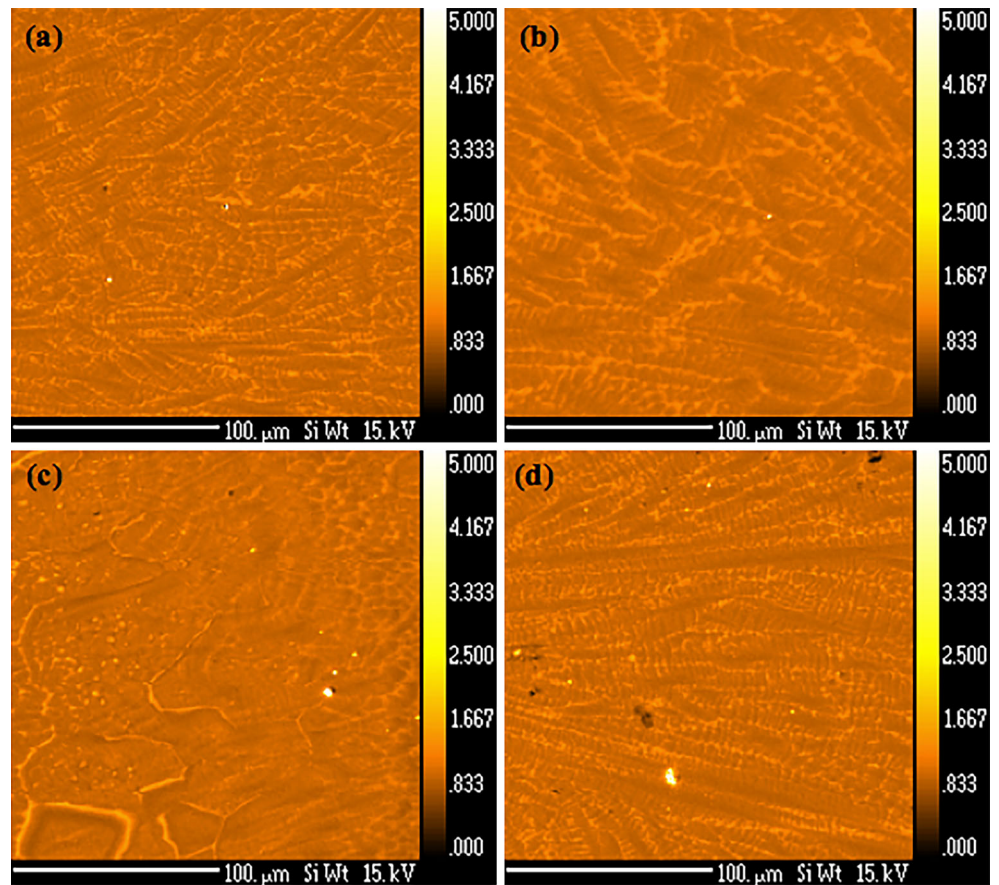




**Fig. 11** Elemental maps of phosphorus taken at the edge of the primary weld nugget **a** sequence 1, **b** sequence 2 (5.7 kA), **c** sequence 3 (6.2 kA) and **d** sequence 4 (6.9 kA)

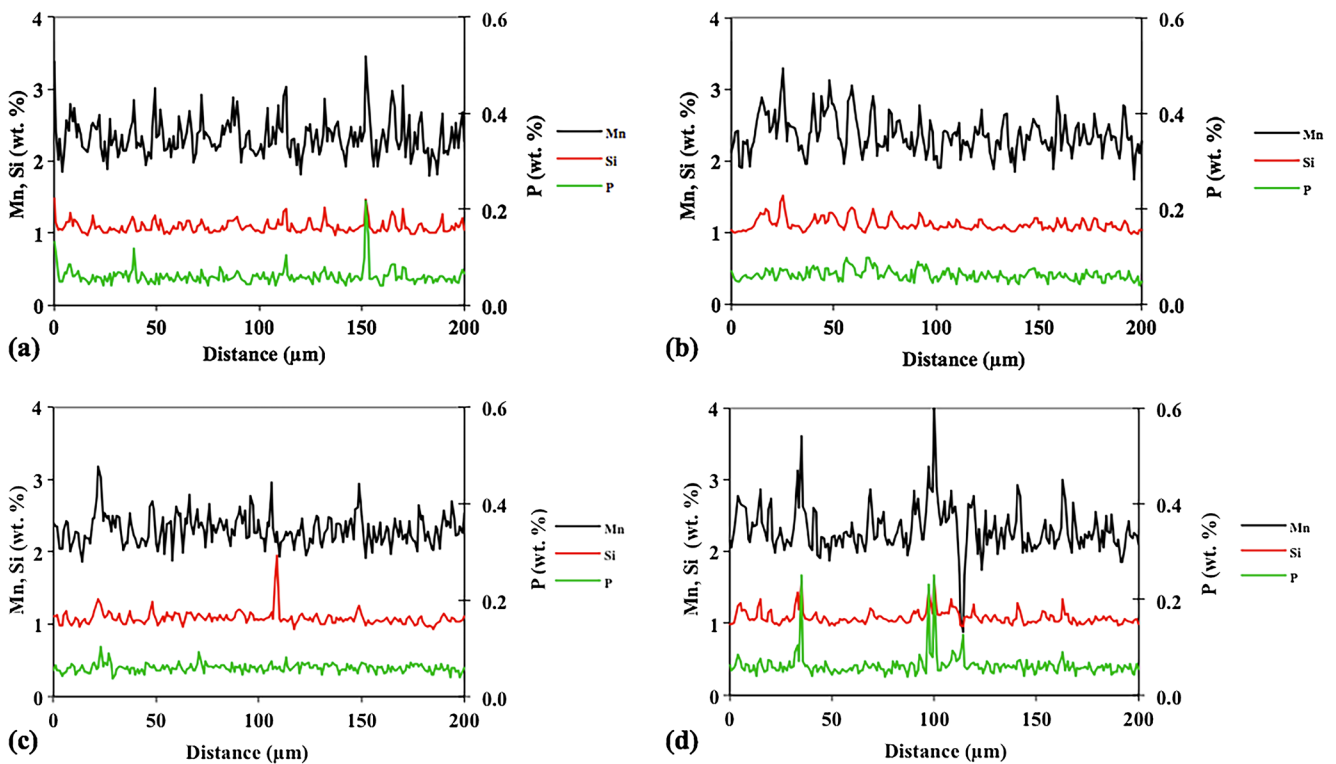
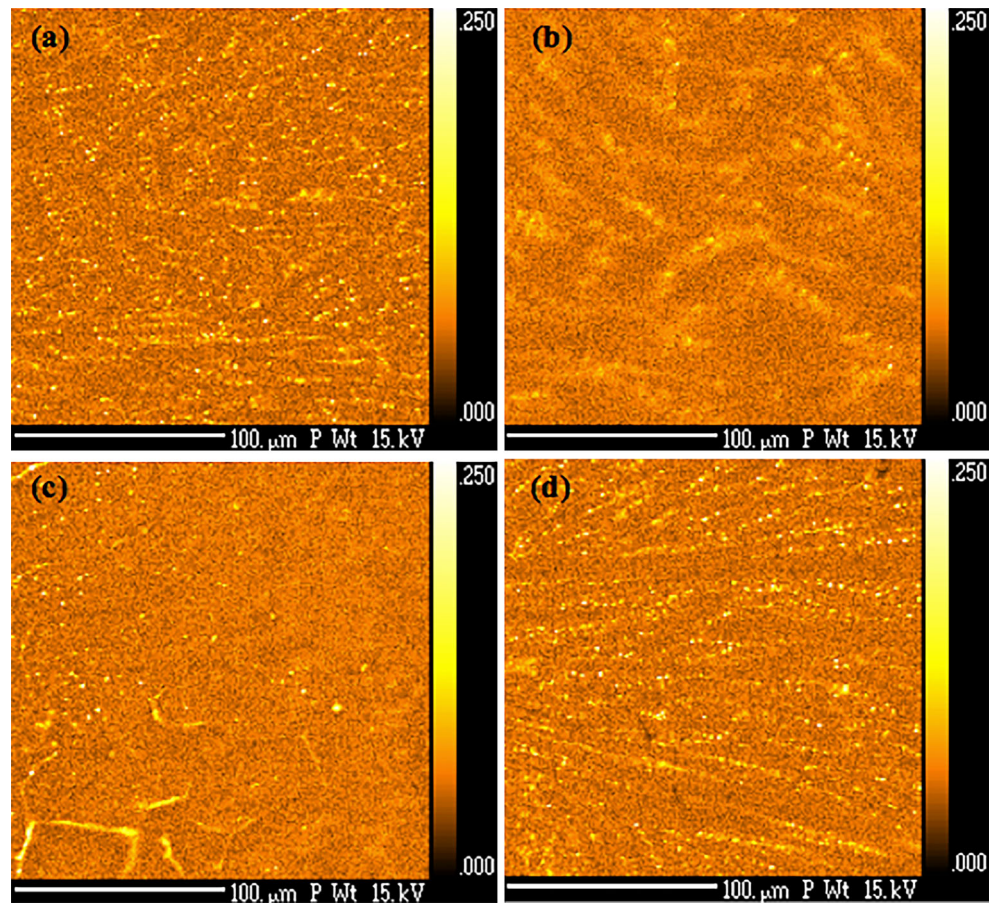


**Fig. 12** Line scans taken vertically at approximately 25  $\mu\text{m}$  from the right-hand side of the elemental plots of **a** sequence 1, **b** sequence 2 (5.7 kA), **c** sequence 3 (6.2 kA) and **d** sequence 4 (6.9 kA)

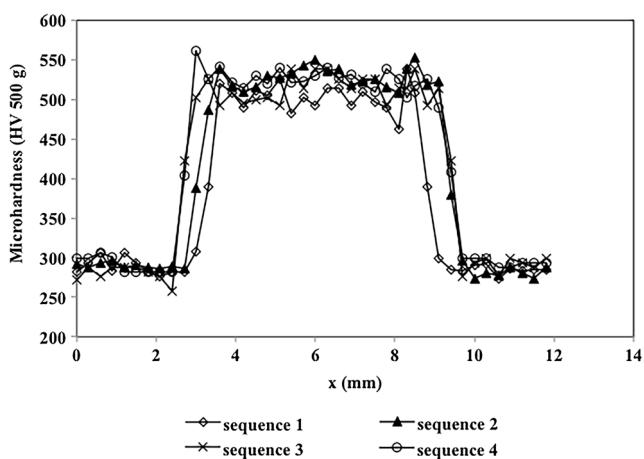
**Table 5** Average compositions and standard deviations obtained from EPMA line scans

	Mn (wt%)		Si (wt%)		P (wt%)	
	Average	Std dev	Average	Std dev	Average	Std dev
Sequence 1	2.340	0.271	1.089	0.085	0.060	0.018
Sequence 2	2.369	0.265	1.116	0.088	0.062	0.011
Sequence 3	2.315	0.214	1.084	0.101	0.059	0.009
Sequence 4	2.309	0.337	1.084	0.098	0.062	0.025

phosphorus occurs. In case of sequence 3, which is welded with two equal pulse currents, the weld edge undergoes the maximum annealing during the second pulse current. The higher current pulse in sequence 3 in comparison with sequence 2 results in a larger grain growth during second current pulse and shows the highest homogenisation of detrimental elements such as phosphorous. The elemental distribution at the weld edge of sequence 4 is similar to sequence 1 (single pulse weld) and shows a dendritic structure that confirms the re-melting of the weld edge during the second pulse current for this weld.

### 4.3 Mechanical properties

During cross tension strength testing, the crack initiates from the weld edge and the microstructure and elemental distribution of this area is of crucial importance. The double pulse RSW improves the cross tension strength of the 3<sup>rd</sup> generation 1 GPa AHSS welds (Fig. 14). The homogenisation of the alloying elements such as phosphorous during the second pulse occurs in the so-called annealed zone and results in improved mechanical performance of the double pulse resistance spot welds. The

**Fig. 13** Microhardness profile of the 3<sup>rd</sup> generation 1 GPa AHSS subjected to the various welding schedules

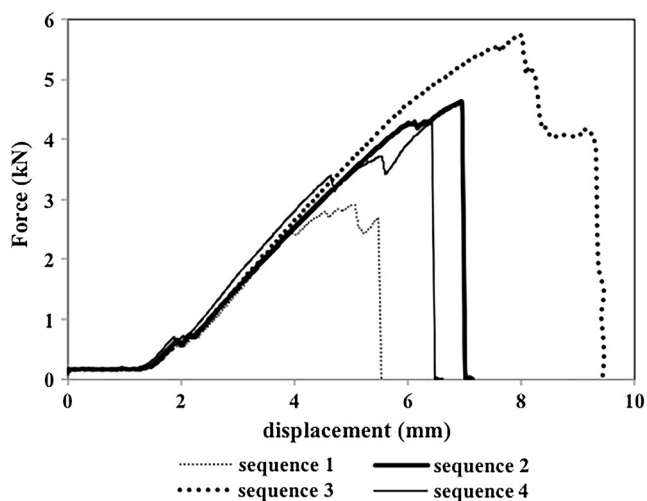
weld subjected to equal pulses (sequence 3) shows the highest cross tension strength.

A higher second pulse current amplitude compared with the first pulse in sequence 4 leads to the formation of a larger secondary weld nugget than sequence 3. The complete primary weld has been re-melted and shows a cast structure, similar to a single pulse weld. The higher cross tension strength of the sequence 4 compared with the sequence 1 is attributed to the larger weld nugget of the double pulse weld (Table 6).

The load-displacement curves show some fluctuations that can be attributed to crack initiation, pop-ins and crack arrest phenomena [24].

A schematic representation of the failure modes for sequences 1–4 is shown in Fig. 15. The failure mode of sequence 3 is a favourable full plug failure (Table 6), which is a significant improvement in the properties of 3<sup>rd</sup> generation 1 GPa AHSS welds.

As weld nugget size is not affected by the secondary current pulses, which are lower than or equal to the primary current amplitude (Tables 4 and 6), the improvement in mechanical properties can be attributed to the microstructural changes and improved homogeneity of alloying elements at the weld edge.

**Fig. 14** Typical force-displacement curves from the cross tension strength (CTS) test on the 3<sup>rd</sup> generation 1 GPa AHSS

**Table 6** Cross tension strength results of the 3<sup>rd</sup> generation 1 GPa AHSS

Sequence	First current (kA)	Second current (kA)	Failure mode	Average weld nugget size (n = 3) (mm)	Average CTS, $F_{CTS}$ (n = 3) (kN)	Average plug ratio (n = 3)	Average displacement at max. force (n = 3) (mm)
1	6.2	–	Interfacial failure	5.1 ± 0.1	2.88 ± 0.08	0%	4.9 ± 0.4
2	6.2	5.7	Partial interfacial failure	5.1 ± 0.1	5.12 ± 0.4	35 ± 4%	7.7 ± 0.8
3	6.2	6.2	Full plug failure	5.2 ± 0.1	5.63 ± 0.2	100%	8.0 ± 0.2
4	6.2	6.9	Partial interfacial failure	5.7 ± 0.2	3.81 ± 0.3	49 ± 2%	6.3 ± 0.5

CTS cross tension strength

## 5 Conclusions

In this research, the effects of a second current pulse during RSW on the microstructure, elemental distribution and mechanical properties of the 3<sup>rd</sup> generation 1 GPa AHSS have been investigated. The following conclusions are derived from the investigation;

1. A second pulse on the 3<sup>rd</sup> generation 1 GPa AHSS welds studied leads to the formation of a secondary weld nugget

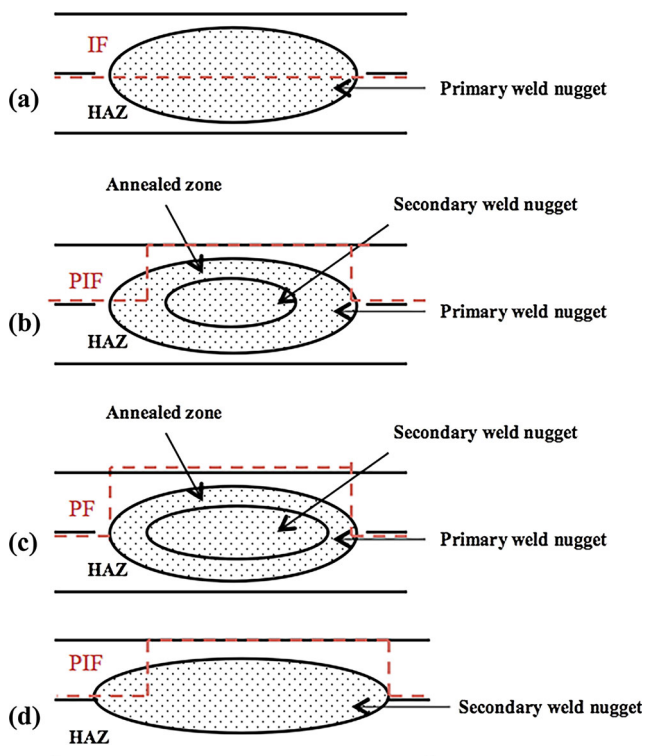


**Fig. 15** Schematic representation of the failures modes for **a** sequence 1 (interfacial failure), **b** sequence 2 (partial interfacial failure), **c** sequence 3 (plug failure) and **d** sequence 4 (partial interfacial failure)

2. A single pulse resistance spot weld shows a typical cast microstructure and low cross tension strength. A lower second pulse current than the first pulse anneals the primary weld nugget at the weld edge and homogenises the alloying elements and as a result improves the cross tension strength. Double pulse welding with equal pulses results in maximum annealing of the primary weld nugget edge, without re-melting the weld edge; therefore, the highest homogenisation of the alloying elements and increase in cross tension strength is obtained for this weld. Higher second pulse current amplitude compared with the first pulse produces a larger weld nugget than the single pulse weld with a similar cast structure and as a result the cross tension strength and displacement is comparable and slightly higher than the single pulse weld.
3. A welding schedule with two equal amplitude pulses induces favourable full plug failure mode for the 3<sup>rd</sup> generation 1 GPa AHSS.

**Acknowledgements** This research was carried out under project number F22.8.13507 in the framework of the Partnership Program of the Materials innovation institute M2i ([www.m2i.nl](http://www.m2i.nl)) and the Foundation of Fundamental Research on Matter (FOM) ([www.fom.nl](http://www.fom.nl)), which is part of the Netherlands Organisation for Scientific Research ([www.nwo.nl](http://www.nwo.nl)). The authors thank Tata Steel for delivering the materials and Mr. Hans Winter for performing the EPMA measurements.

**Open Access** This article is distributed under the terms of the Creative Commons Attribution 4.0 International License (<http://creativecommons.org/licenses/by/4.0/>), which permits unrestricted use, distribution, and reproduction in any medium, provided you give appropriate credit to the original author(s) and the source, provide a link to the Creative Commons license, and indicate if changes were made.

## References

1. Keeler S (2015) Advanced high strength steels (AHSS) guidelines. Technical Report Version 4.1, World auto steel, World steel association
2. Khanna SK, Long X (2008) Residual stresses in resistance spot welded steel joints. *Sci Technol Weld Join* 13(3):278–288
3. Nayak SS, Zhou Y, Baltazar Hernandez VH, Biro E (2012) Resistance spot welding of dual-phase steels: heat affected zone softening and tensile properties. *Proceedings of the 9th International Conference on Trends in Welding Research*, Chicago, Illinois, United States: 641–649
4. Janota M, Neumann H (2007) Share of spot welding and other joining methods in automotive production. IIW Annual Assembly, Dubrovnik, Croatia, document number: III- 1423-07
5. Den Uijl NJ, Smith S (2006) Resistance spot welding of advanced high strength steels for the automotive industry. 4th International Seminar on Advances in Resistance Welding, Wels, Austria: 30–60
6. Amirthalingam M, van der Aa EM, den Uijl NJ, Hermans MJM, Richardson IM (2012) Phosphorous and boron segregation during resistance spot welding of advanced high strength steels. *Proceedings of the 9th International Conference on Trends in Welding Research*, Chicago, Illinois, United States: 217–226
7. Amirthalingam M, van der Aa EM, Kwakernaak C, Hermans MJM, Richardson IM (2015) Elemental segregation during resistance spot welding of boron containing advanced high strength steels. *Weld World* 59:743–755
8. Amirthalingam M (2010) Microstructural development during welding of TRIP steels. Dissertation, Delft University of Technology
9. Grajcar A, Rozanski M, Kaminska M, Grzegorzczak B (2014) Study on non-metallic inclusions in laser-welded TRIP-aided Nb-microalloyed steel. *Arch Metall Mater* 59:1163–1169
10. Ramirez JE (2008) Characterization of high-strength steel weld metals: chemical composition, microstructure, and non-metallic inclusions. *Weld J* 87:65s–75s
11. Den Uijl NJ, Smith S, Moolevliet T, Goos C, van der Aa EM, van der Veldt T (2008) Failure modes of resistance spot welded advanced high strength steels. 5th International Seminar on Advances in Resistance Welding, Toronto, Canada
12. Pouranvari M, Marashi SPH (2013) Critical review of automotive steels spot welding: process, structure and properties. *Sci Technol Weld Join* 18(5):361–403
13. Den Uijl NJ, Nishibata H, Smith S, Okada T, Uchihara M, Fukui F (2007) Prediction of post weld hardness of advanced high strength steels for automotive application using a dedicated carbon equivalent number. IIW Annual Assembly, Dubrovnik, Croatia, document number: III- 1444-07
14. Van der Aa EM, Amirthalingam M, Winter J, Hanlon DN, Hermans MJM, Rijnders M, Richardson IM (2015) Improved resistance spot weldability of 3rd generation AHSS for automotive applications. 11th International Seminar on Numerical Analysis of Weldability, Graz, Austria
15. Baltazar Hernandez VH, Okita Y, Zhou Y (2012) Second pulse current in resistance spot welded TRIP steel—effects on the microstructure and mechanical behavior. *Weld J* 91:278s–285s
16. Matsushita M, Taniguchi K, Oi K (2013) Development of next generation resistance spot welding technologies. JFE Technical Report 18
17. Den Uijl NJ (2015) Resistance spot welding of advanced high strength steels. Dissertation, Delft University of Technology
18. Sawanishi C, Ogura T, Taniguchi K, Ikeda R, Oi K, Yasuda K, Hirose A (2014) Mechanical properties and microstructures of resistance spot welded DP980 steel joints using pulsed current pattern. *Sci Technol Weld Join* 19(1):52–59
19. Peer A, Lu Y, Abke T, Kimchi M, Zhang W (2016) Deformation behaviors of subcritical heat-affected zone of ultra-high strength steel resistance spot welds. 9th International Seminar and Conference on Advances in Resistance Welding. Miami, USA
20. Lu Y, Peer A, Abke T, Kimchi M, Zhang W (2016) Heat-affected zone microstructure and local constitutive behaviors of resistance spot welded hot-stamped steel. *Sheet Metal Welding Conference XVII*. Livonia, MI
21. SEP 1220-2 (2007) Testing and documentation guideline for the joinability of thin sheet of steel—part 2: resistance spot welding. Technical Report 08, VDEh standard
22. Eftekharamilani P, Van der Aa EM, Amirthalingam M, Hermans MJM, Richardson IM (2016) Effect of double pulsing on the microstructural evolution of low alloyed and 3rd generation 1 GPa advanced high strength steels during resistance spot welding. 9th International Seminar and Conference on Advances in Resistance Welding, Miami, USA
23. Furusako S, Murayama G, Oikawa H, Nose T, Watanabe F, Hamatani H, Takahashi Y (2013) Current problems and the answer techniques in welding technique of auto bodies (first part)—Nippon Steel Technical Report 103: 69–75
24. Krajcarz F, Lorenzon AFG, Lucas E, Pineau A (2013) Fracture toughness of the molten zone of resistance spot welds. *Int J Fract* 181:209–226